Search and study of young infrared stellar clusters

N. Azatyan *

Byurakan Astrophysical Observatory, 0213 Aragatsotn Prov., Armenia

Abstract

The "bricks" of the Galactic disc are giant molecular clouds, which are birthplaces of stellar population. Therefore, there is a genetic connection between young stellar objects (YSOs) and their surrounding Interstellar Medium (ISM). The thesis is devoted to a search for young stellar clusters in the vicinity of IRAS sources and a detailed study of three selected star-forming regions: IRAS 05137+3919, 05168+3634, and 19110+1045, which includes determining the parameters of the ISM based on far-infrared data, the identification and classification of YSOs using color-color and color-magnitude diagrams, the modeling of stellar parameters, and the construction and interpretation of the luminosity functions. It is likely that the three young stellar clusters were formed under different scenarios. The age spread of the IRAS 05137+3919 and IRAS 05168+3634 regions is much larger, and, therefore, we concluded that the stellar population is formed as a result of independent condensations. The age spread of the IRAS clusters' members in the third region, which is a pair of ultra-compact HII regions (UCHIIs), namely G45.12+0.13 and G45.07+0.13, is small. The small age spread suggests that the clusters may originate from a single triggering event. Moreover, high-mass YSOs were obtained only in the G45.07+0.13 and G45.12+0.13 UCHII regions where the ISM initial density was higher and the star formation proceeded relatively quickly.

Keywords: *stars: pre-main sequence – Stars: luminosity function – Infrared: stars – radiative transfer*

1. Introduction

The star formation process continues at all stages of the evolution of our and other galaxies, including the present stage (Ambartsumian, 1947), and is one of the most important processes which provides the observational output of the galaxies. The "bricks" of the Galactic disc are giant molecular clouds, which are birthplaces of stellar population. There is a large number of observation data, which witness that the star formation process has consecutive nature (Soderblom, 2010). Therefore, the spatial distribution of YSOs in clusters and the quantitative ratio between YSOs with different masses and ages are essential for understanding the evolutionary history of a cluster itself. However, such studies have been seriously hampered by the fact that galactic clusters form in giant molecular clouds and during their formation and earliest stages of evolution are completely embedded in molecular gas and dust, and thus obscured from view. During the last two decades, the development of infrared (IR) astronomy has dramatically improved this situation providing astronomers the ability to survey and systematically study embedded clusters within molecular clouds.

Embedded stellar clusters, which are still surrounded by their progenitor molecular clouds are of particular interest to understand which properties of stellar clusters are related to their origins and which are derived from subsequent evolution (Lada & Lada, 2003). There is also a certain relationship between the properties of the stellar population of young clusters and the process of their formation. If the star-formation in clusters is triggered, the age spread of stars in the cluster should be small, while in self-initiated protocluster condensations, the individual clumps should have a larger age spread (e.g. Preibisch, 2012).

Nowdays, it is known that there is a genetic connection between YSOs and their surrounding ISM. Consequently, the study of ISM in conjunction with the study of embedded in them YSOs is very important for understanding the process of formation and evolution of the stellar population in galaxies (e.g. González-Samaniego & Vazquez-Semadeni, 2020). This necessitates an integrated approach to study of star-forming regions, which implies a determination and detailed study of the main properties of already formed young
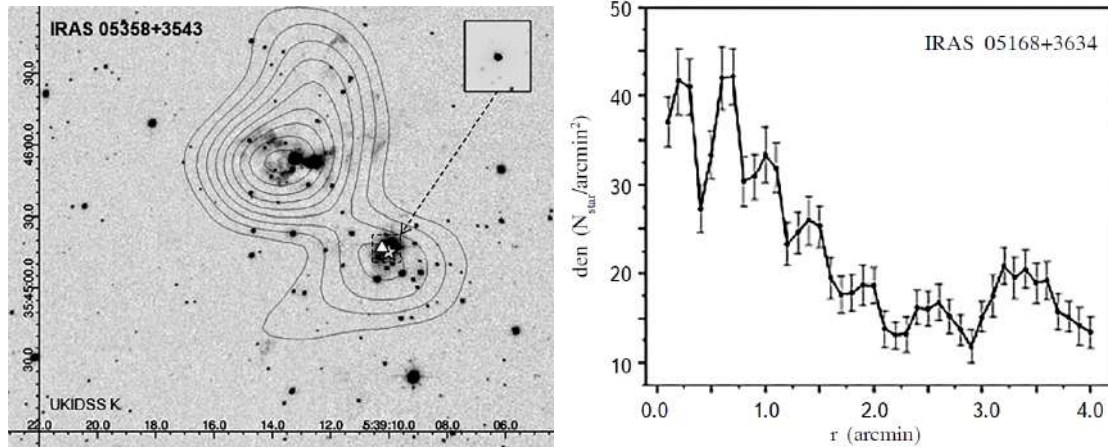
---

*nayazatyan@bao.sci.am

Figure 1. (*Left*) NIR images and isodenses of IRAS 05358+3543 star-forming region. IRAS and MSX sources are indicated by stars and triangles, respectively. (*Right*) Radial distribution of the stellar density relative to IRAS 05168+3634 source. Vertical lines are standard errors.

stellar clusters (density, mass function, evolutionary age distribution, etc.) and the environment (density, temperature, etc.). This approach was taken in this work.

The thesis presents the results of both a search for young stellar clusters in the vicinity of IRAS sources and a detailed study of three selected star-forming regions: IRAS 05137+3919, 05168+3634, and 19110+1045. The main selection criteria of these three regions are their considerable extent and multi-component complex structure, which implies the presence of several local nests of star formation. Besides, the preliminary studies have shown that the star-forming regions differ in their stellar composition and structural properties. All three regions, however, despite their certain differences, are united by one aspect - they are regions of active star formation. For all regions a detailed study was conducted, which includes the following topics: 1) determination of the parameters of ISM, namely the distribution of $N(H_2)$ hydrogen column density and T_d dust temperature; 2) the search for young stellar clusters; 3) identification of the clusters' members using their infrared properties; 4) investigation of the structural properties of the young stellar clusters; 5) determination of the age and age spread of the clusters' members; 6) construction of the Luminosity Functions and Mass Functions for the clusters. This thesis is based on the papers Azatyan (2019), Azatyan & Nikoghosyan (2018), Azatyan et al. (2016, 2020, 2022), Nikoghosyan & Azatyan (2014), Nikoghosyan et al. (2020, 2021).

We have organised the paper as follows. Section 2 describes the used data; in Section 3 we present the methods; in Section 4, we analyse the stellar population in the regions. Finally, the study results are summarised in Section 5.

2. Used data

We used data covering a wide range of near- to far-infrared (NIR, FIR) wavelengths. The first dataset is the archival NIR photometric data in the J, H, and K bands of the Galactic Plane Survey DR6 (UKIDSS GPS, Lucas et al., 2008) with a resolution of $0.1''$/px, which is one of the five surveys of the UKIRT Infrared Deep Sky Survey (UKIDSS). This survey is complete to approximately 18 mag in the K band and provides a percentage probability of an individual object being a star, galaxy, or noise. In the absence of UKIDSS GPS data, we used the data of the Two Micron Sky Survey (2MASS, Cutri et al., 2003).

Archival MIR observations were obtained from the Spitzer Space Telescope under the Galactic Legacy Infrared Midplane Survey Extraordinaire (GLIMPSE) and GLIMPSE 360 programs (Churchwell et al., 2009). GLIMPSE observations were taken using the *Spitzer* Infrared Array Camera (IRAC, Fazio et al., 2004) centred at approximately 3.6, 4.5, 5.8, and 8.0 μm with a resolution of $0.6''$/px. At longer wavelengths, we used data from a survey of the inner Galactic plane using the Multiband Infrared Photometer for *Spitzer* (MIPSGAL). The survey field was imaged in 24 and 70 μm passbands with resolutions of $6''$/px and $18''$/px, respectively (Carey et al., 2009); however, only 24 μm data were available for the studied star-forming regions.

We also used Wide-field Infrared Survey Explorer (WISE, Wright et al., 2010) data in the 3.4, 4.6, 12, and 22 μm bandpasses. We used the Midcourse Space Experiment (MSX, Price et al., 2001) full plane
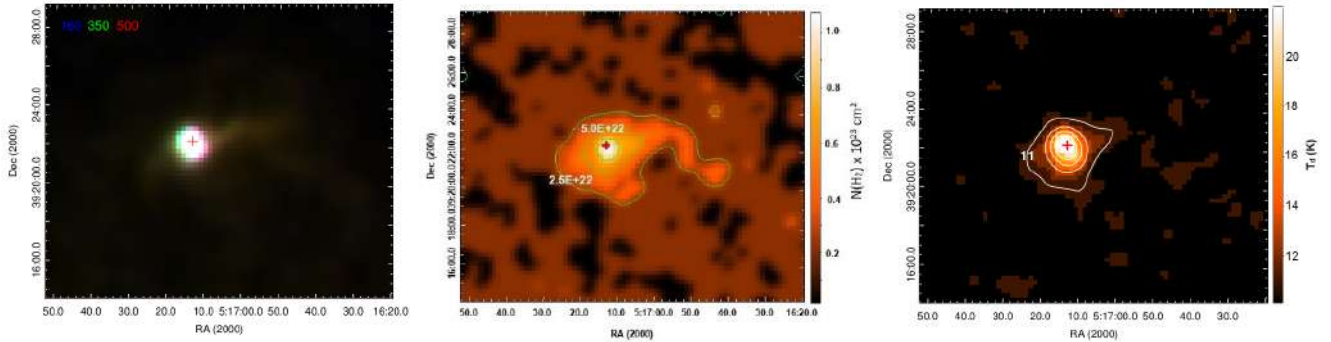
Figure 2. (*Left*) Colour-composite image of IRAS 05137+3919 star-forming region: 160 μm (blue), 350 μm (green), and 500 μm (red). (*Middle*) Column density map of the region. The external isodense corresponds to the 2.5x10^{22} cm^{-2} value and the interval between isodences is also 2.5x10^{22} cm^{-2}. (*Right*) Dust temperature of the region. The external isotherm corresponds to 11 K and interval between isotherms is 2.5 K. The position of the IRAS source is indicated by red cross.

survey data in the 8.28, 12.13, 14.65, and 21.3 μm bands.

To study gas and dust, as well as deeply embedded point sources, we used FIR observations, in the 70–500 μm range, obtained with the Photodetector Array Camera and Spectrometer (PACS, Poglitsch et al., 2010) and the Spectral and Photometric Imaging Receiver (SPIRE, Griffin et al., 2010) on board the 3.5 m *Herschel* Space Observatory (Pilbratt et al., 2010). For our analyses, we used photometric data and images from the PACS 70 and 160 μm catalogues, in addition to *Herschel* infrared Galactic Plane Survey (Hi-GAL, Molinari et al., 2016) data at 70, 160, 250, 350, and 500 μm. The corresponding Herschel half-power beamwidth (HPBW) values are 5.0″ at 70 μm, 11.4″ at 160 μm, 17.8″ at 250 μm, 25.0″ at 350 μm, and 35.7″ at 500 μm. The Infrared Astronomical Satellite (IRAS, Neugebauer et al., 1984) Point Source Catalog v2.1 (PSC) data was used. The IRAS mission performed an unbiased, sensitive all-sky survey at 12, 25, 60, and 100 μm. *Herschel* PACS and Hi-GAL data have better resolution than the IRAS PSC data. Therefore, we used the data from the Hi-GAL 70, 160 μm, or *Herschel* PACS 70, 160 μm catalogs instead of IRAS 60 and 100 μm data.

3. Methods

The thesis contains two main scientific directions, namely study of ISM and YSOs. To study gas and dust, as well as deeply embedded point sources, we used FIR observations in the 70–500 μm range since this wavelength range covers the peak of the spectral energy distribution of cold dust emission. Modified single-temperature blackbody fitting was subsequently carried out to obtain the important ISM parameters such as the hydrogen column density (N(H$_2$)) and the dust temperature (T$_d$).

To select and study the potential stellar members of the star-forming regions, we used NIR, mid-infrared (MIR), and FIR data. The identification of stellar objects was performed with GPS UKIDSS-DR6 as the main catalogue, and then other MIR and FIR catalogues were cross-matched with it within 3 σ of the combined error–matching radius. We selected objects with a $< 30\%$ probability of being noise and a magnitude of K < 18.02 mag, taking into account the K band limit of the UKIDSS survey. In addition, we removed objects with zero errors of measured magnitudes in the J, H, and K bands. Since, the presence of circumstellar discs and envelopes cause an IR excess of a YSO, therefore YSO candidates were identified based on their position in colour–colour (c-c) IR diagrams. The choice of colours depends on the available data. To confirm the selected YSOs and to determine their parameters, we constructed their SEDs and fitted them with the radiative transfer models of Robitaille et al. (2007).

4. Results and Discussion

4.1. Selection of the regions

At first, we carried out the search and study of compact clusters in 20 star-forming regions from the list of Varricatt et al. (2010). In order to detect clusters and to refine their sizes in considered 20 regions,
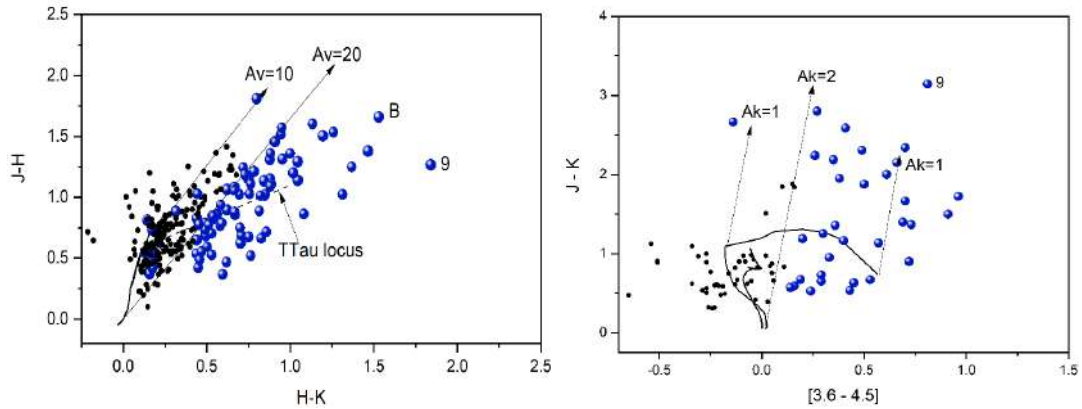
Figure 3. (*Left*) (J-H) vs. (H-K) and (*Right*) (J-K) vs. [3.6]-[4.5] c-c diagrams for IRAS 05137+3919 star-forming region. Not all non-classified objects (black circles) are presented in these diagrams. Southwest component B of CPM 15 YSO and the reddest object with number 9 are labeled.

we constructed surface and radial stellar density distribution and around each IRAS source using NIR and MIR photometric data. Figure 1 shows the examples of surface stellar density distribution map (left panel) and radial density distribution of stars (right panel) in two different star-forming regions. We have also compared the LF of the stellar objects in the clusters and their fields using the Kolmogorov-Smirnov test. We were able to detect compact clusters in 12 and 4 regions based on NIR and MIR data, respectively. This represents 80% of the overall number of regions that were studied and is substantially higher than the results based on data from the 2MASS.

4.2. Regions for detail study

Among above mentioned 16 identified clusters, we selected three star-forming regions for a detailed study, namely IRAS 05137+3919, 05168+3634, and 19110+1045, which includes the study of both the stellar population and the ISM. The main selection criteria of these three regions are their considerable extent and multicomponent complex structure, which implies the presence of several local nests of star formation. The regions are little studied, but at the same time, there is sufficient observational data for their detailed study. Besides, our preliminary studies have shown that the star-forming regions differ in their stellar composition and structural properties. These star-forming regions are also of interest because they are located at large distances, which will allow us to test the capabilities of the databases at our disposal. All three regions, despite their certain differences, are united by one aspect - they are regions of active star formation.

A young stellar cluster located in the vicinity of IRAS 05137+3919 associated with the CPM 15 YSO. Different manifestations of active star formation have been observed in this region, such as maser emissions, as well as CO and H_2 outflows. Left panel of Figure 2 shows the colour-composite image covering the IRAS 05137+3919 star-forming region. The region stands out sharply in terms of brightness. Using the modified single-temperature blackbody fitting, we have determined the main parameters ($N(H_2)$ and T_d) of cold composing gas-dust matter in the region and their maps are presented in the middle and right panels of Figure 2. The $N(H_2)$ and T_d maps show that the star-forming region stands out sharply in terms of brightness with a relatively high density and temperature. The maxima of both $N(H_2)$ ($\sim 1.0 \times 10^{23}\,cm^{-2}$) and T_d (22 K) almost coincide with position of the IRAS source. Towards the periphery, both parameters decrease up to $2.2 \times 10^{22}\,cm^{-2}$ and 11 K.

The radial distribution of stars density relative to the position of IRAS 05137+3919 confirmed the existence of a cluster in the vicinity of the IRAS source with 1.5′ radius. Within this radius, the stellar density (38 stars/arcmin^2) is twice the density of the field (19 stars/arcmin^2).

The selection of YSOs in the IRAS 05137+3919 star-forming region was based on two c-c diagrams, namely (J-H) versus (H-K) and (J-K) versus [3.6]-[4.5]. Figure 3 (left and right panels) shows the positions of 253 objects located within 1.5′ radius relative to the IRAS 05137+3919 source. Totally, we selected 84 YSOs (blue circles) based on these two c-c diagrams. This is almost 1.5 times greater than the earlier estimate of the cluster members (Faustini et al., 2009). Since stellar magnitudes in the *Spitzer* 3.6 and 4.5 μm bands are available for only 33 YSOs, we were able to obtain parameters of these YSOs using the SED fitting tool. The full tables of selected YSOs with their parameters are included in the thesis. The
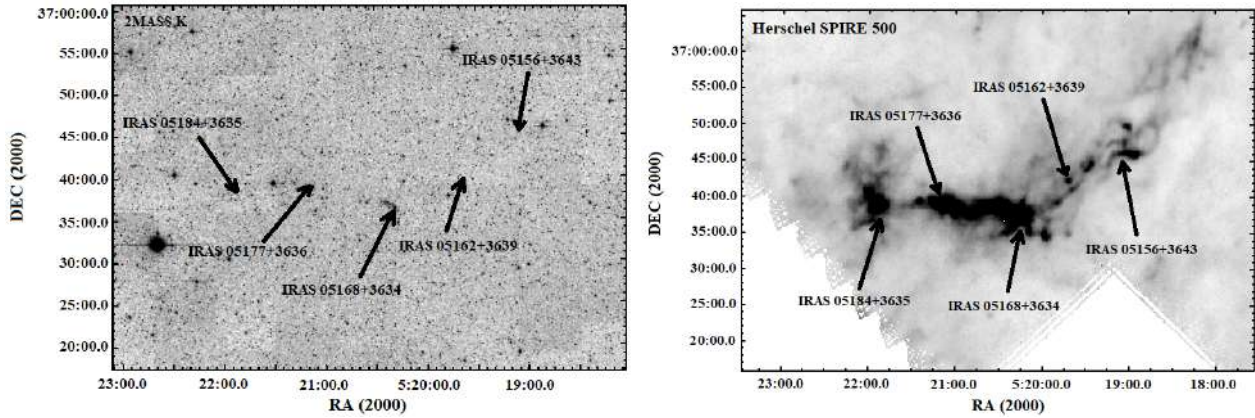
Figure 4. The IRAS 05138+3634 star-forming region at (*left*) NIR (2MASS K-band) and (*right*) FIR (*Herschel* SPIRE 500 μm) wavelength ranges. The positions of five IRAS sources are indicated by arrows.
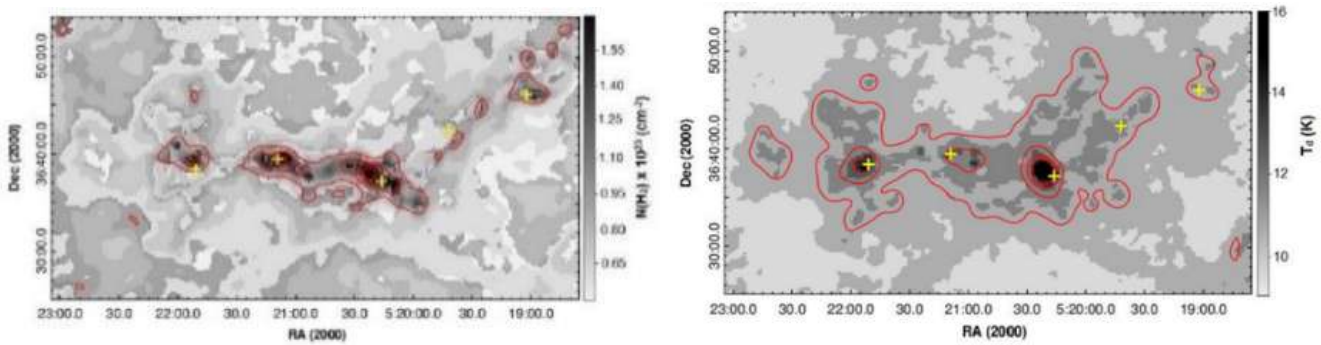

Figure 5. Maps of N(H$_2$) column density (*left*) and T$_d$ dust temperature (*right*) of IRAS 05168+3634 star-forming region. The outer isodense on the N(H$_2$) map corresponds to 0.9×10^{23} cm^{-2}, and the interval between isodenses is $\sim 0.4 \times 10^{23}$ cm^{-2}. The outer isotherm on the T$_d$ map corresponds to 11 K, and the interval between isotherms is 1 K. The positions of IRAS sources are marked by yellow crosses.

selected YSOs are distributed nonuniformly in the star-forming region and form two subgroups; one is located around CPM 15, while the second group contains a significant number of middle-mass objects surrounded by gas-dust nebulae.

The distribution of 33 identified YSOs in colour-magnitude diagram (CMD) and histograms of their evolutionary ages clearly showed very wide spread. On the basis of these, it can be assumed that, in general, the star formation process in the considered region is sequential. In addition, based on K luminosity function (KLF) slope, the age of IRAS 05137+3919 star-forming region is estimated between 0.1 and 3 Myr. Therefore, the large age spread of IRAS 05137+3919 star-forming region give us bases to conclude that the stellar population is formed as a result of independent condensations in the parent molecular cloud.

Next young stellar cluster is located in the vicinity of IRAS 05168+3634 source. The presence of different maser emissions and ^{13}CO cores confirms its active star-forming nature. The region has a more complicated structure in the FIR wavelengths than in the NIR (see Figure 4). The complex structure of the region is clearly visible in FIR (right panel). Moving toward longer wavelengths, the cloud filaments surrounding IRAS 05168+3634 become more visible and it is obvious that the IRAS 05168+3634 star-forming region is more extended and is located within a 24 arcmin radius molecular cloud. Studying the common star-forming region in the molecular cloud, it turns out that apart from IRAS 05168+3634, there are four IRAS sources (IRAS 05184+3635, 05177+3636, 05162+3639, and 05156+3643) embedded in the same molecular cloud. Since, the distribution of stars in our field is 35 times different from the homogeneous distribution and their distribution in the field repeats the shape of the molecular cloud seen in FIR wavelengths, we concluded with a high probability that all five IRAS star-forming regions are at the same distance.

The N(H$_2$) and T$_d$ maps in the left and right panels of Figure 5 show that the star-forming region clearly stands out against the background of the surrounding molecular cloud both with a higher density and temperature. The relatively hotter gas-dusty matter forms dense condensations around the IRAS objects. An exception is the IRAS 05162+3639 sub-region, near which on the N(H$_2$) map there is practically no

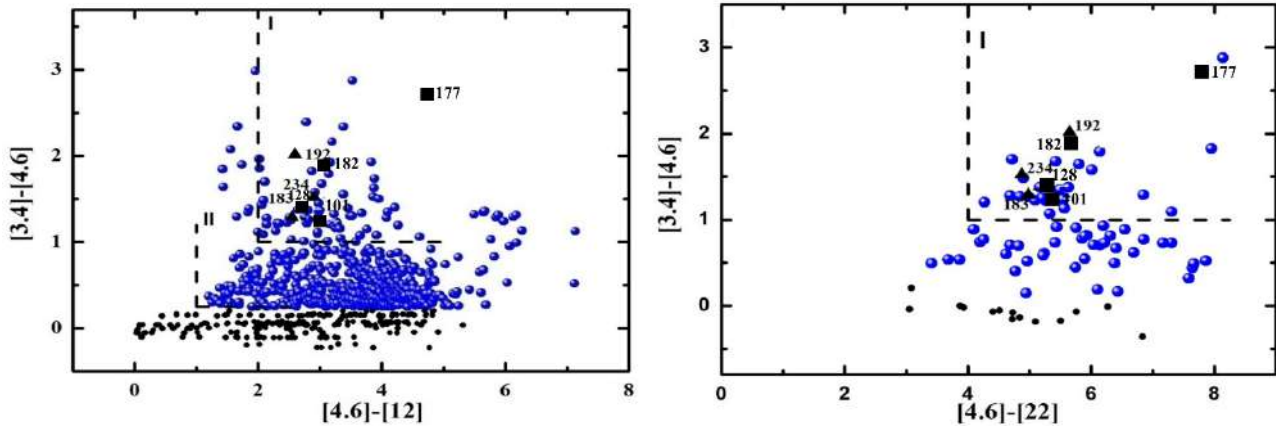Figure 6. [3.4]–[4.6] vs. [4.6]–[12] (*left*) and [3.4]–[4.6] vs. [4.6]–[22] (*right*) c-c diagrams for the IRAS 05168+3634 star-forming region. The blue circles are selected YSOs and black circles are unclassified ones. Not all unclassified objects are presented in these diagrams. IRAS and MSX sources are indicated by triangles and squares, respectively, and they are labeled.

region with a relatively higher density and no group of YSOs has been identified around this source, but only 5 stars. In general, in the whole star-forming region T_d varies from 11 to 24 K, and $N(H_2)$ - from $\sim$1.0 to 4.0×10^{23} cm^{-2}.

The selection of YSOs in the IRAS 05168+3634 star-forming region was based on four c-c diagrams, namely (J-H) versus (H-K), K-[3.6] versus [3.6]-[4.5], [3.4]-[4.6] versus [4.6]-[12], and [3.4]-[4.6] versus [4.6]-[22]. Figure 6 shows only two of these c-c diagrams. We added to our list those objects classified as YSOs in at least two c-c diagrams. Totally, we selected 1224 YSOs within a 24 arcmin radius. The distribution of classified YSOs in the field showed that Class II objects are distributed more homogeneously on the field than Class I objects, which are located in certain areas and show clear concentrations with sub-structures. This confirms the assumption that, unlike the Class II objects, Class I objects did not have enough time to leave their birthplaces after formation. Since the region is quite large, further investigations have only been performed on concentration areas. We estimated the size of each concentration in the molecular cloud based on map of the distribution of stellar surface density. Then, 240 YSOs of 1224 selected from c-c diagrams within the determined radii were explored in greater detail. The full tables of 240 selected YSOs with their NIR, MIR and FIR photometry and parameters (only 120 YSOs) obtained by SED fitting tool are available VizieR On-line Data Catalog[1].

The distribution of selected YSOs in K versus J-K CMDs and histograms of their evolutionary ages clearly showed very wide spread as in IRAS 05137+3919 case. KLF slopes suggested that the age of all four subregions (except IRAS 05162+3639) can be estimated between 0.1 and 3 Myr. In the case of the IRAS 05162+3639 subregion, there are not enough YSOs to construct the KLF. Therefore, the large age spread of IRAS 05168+3634 star-forming region give us bases to conclude that the stellar population is formed as a result of independent condensations in the parent molecular cloud.

Since, the results for the distance of IRAS 05168+3634 star-forming region are quite different (1.88 and 6.1 kpc), we attempt to identify the list of YSOs in the *Gaia* EDR3 database. In total, we were able to identify 65 objects, but only for 11 of them (located in all five sub-regions) the parallax measurement accuracy is high enough ($\overline{\omega}/\sigma_{\overline{\omega}} > 5$) and such a small number of objects is quite expected since YSOs are embedded in a dense ISM. The result obtained from *Gaia* EDR3 data can be considered as one more argument in favor of the fact that all sub-regions are embedded in the single molecular cloud and belong to the same star-forming region, which is located at $\sim$1.9 kpc distance.

The last star-forming region is associated with IRAS 19110+1045 and 19111+1048 sources, referred to as G45.07+0.13 and G45.12+0.13 UCHII regions, respectively. This complex is an ideal laboratory to investigate the early stages of massive star formations and their influence on natal environments. Figure 7 presents colour-composite images covering the molecular cloud. The G45.12+0.13 and G45.07+0.13 UCHII regions stand out sharply in terms of brightness. The images also indicate that the UCHII regions are connected by a relatively colder bridge and are thus very likely a physically bound system.

The $N(H_2)$ and T_d maps of the wider region surrounding the G45.12+0.13 and G45.07+0.13 UCHII

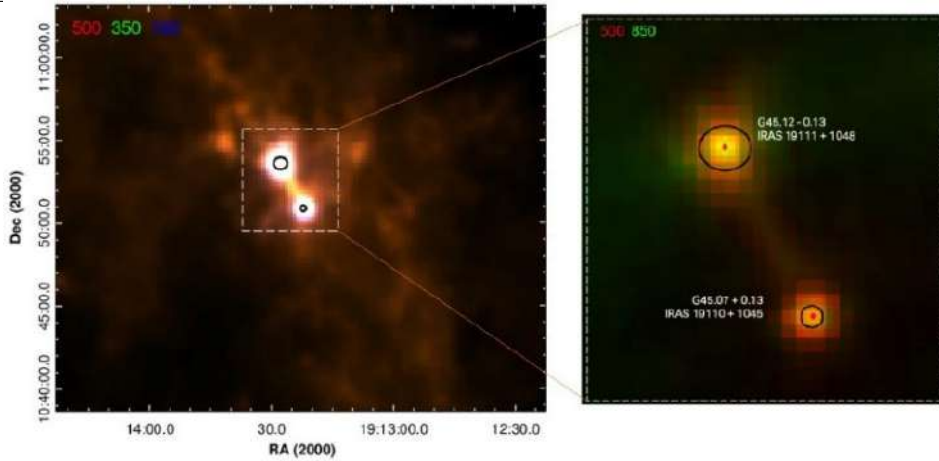[1] The full tables are available in VizieR On-line Data Catalog: J/A+A/622/A38

Figure 7. Colour-composite images of G45.12+0.13 and G45.07+0.13 UCHII regions. Left panel: *Herschel* 160 μm (blue), 350 μm (green), and 500 μm (red); right panel: zoomed area (white dotted square) at SCUBA 850 μm (green) and *Herschel* 500 μm (red). The positions and dimensions of the radio sources are marked by black circles. A red dot represents the position of an IRAS source.
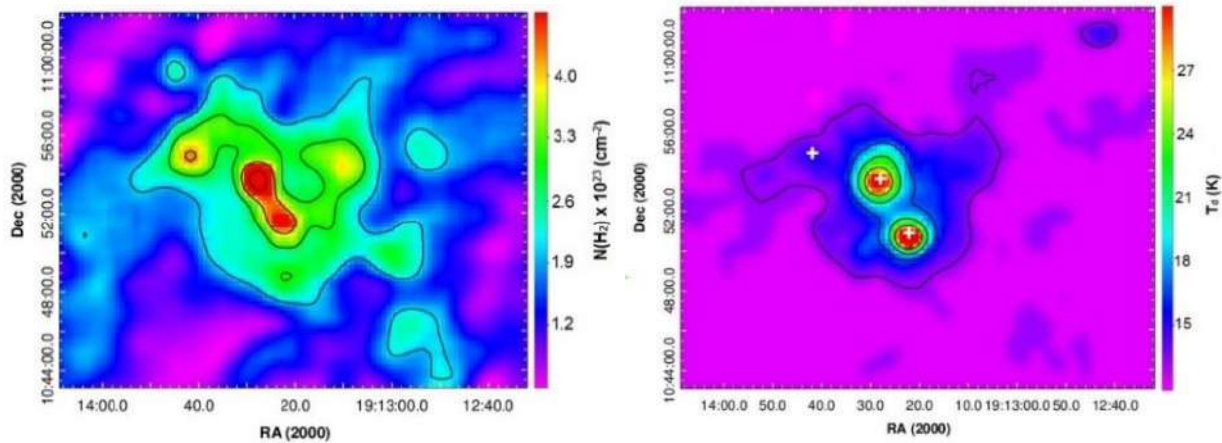

Figure 8. Maps of N(H$_2$) column density (*left*) and T$_d$ dust temperature (*right*) of the region surrounding G45.12+0.13 and G45.07+0.13 UCHII objects. The outer isodense corresponds to 2.0x10^{23} cm^{-2} and interval between isodenses is 1.0x10^{23} cm^{-2}. The outer isotherm corresponds to 13 K and the interval between isotherms is 4 K. The positions of the IRAS and BGPC 6737 sources are marked by white crosses.

objects are shown in Figure 8. Both UCHII regions are distinct from the molecular cloud due to their high dust temperature and column density with an almost spherically symmetric distribution. This is fully consistent with the basic concept of UCHII regions about the presence of a hot, high mass stellar source and stellar wind, which leads to the blowing out of matter (Stahler & Palla, 2005). In general, within both regions, T$_d$ varies from about 17 to 40 K and N(H$_2$) varies from about 3.0 to 5.5x10^{23} cm^{-2}. T$_d$ drops significantly from the centres to the periphery, reaching a value of about 18–20 K. In G45.07+0.13 region, the IRAS source is somewhat offset from the density maximum. Near IRAS 19110+1045, the column density is ∼3.5x10^{23} cm^{-2}. The IRAS source is located close to the dust temperature maximum (T$_d$ = 42 K). In G45.12+0.13 region, the position of IRAS 19111+1048 coincides with the maxima of both the column density (5.5x10^{23} cm^{-2}) and temperature (35 K). The isotherms are slightly elongated towards the northwest, which may relate to the presence of two UCHIIs (G45.12+0.13 and G45.13+0.14). The presence of a region (bridge) with relatively high density (N(H$_2$) ≈ 4.3x10^{23} cm^{-2}) and low temperature (T$_d$ ≈ 19 K) positioned between the two UCHII regions suggests that they are physically connected.

The selection of YSOs in the IRAS 19110+1045 and 19111+1048 star-forming regions was based on six c-c diagrams, namely (J-H) versus (H-K), K-[3.6] versus [3.6]- [4.5], [3.6]-[4.5] versus [5.8]-[8.0], [3.6]-[5.8] versus [8.0]-[24], [3.4]-[4.6] versus [4.6]-[12], and [3.4]-[4.6] versus [4.6]-[22]. Figure 9 shows only two of these c-c diagrams. We added to our list those objects classified as YSOs in at least two c-c diagrams. However, since the region has two saturated areas in the MIR band around the IRAS sources (IRAS 19110+1045
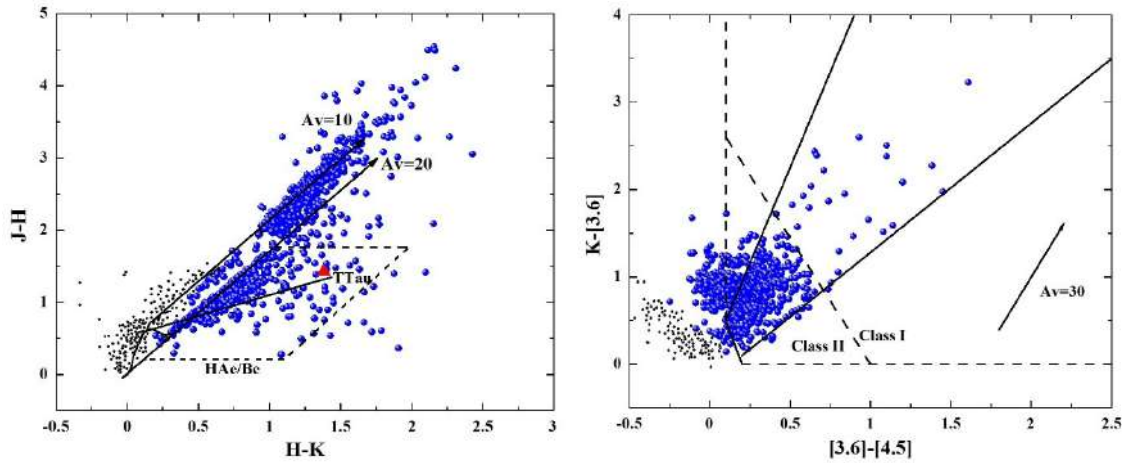
Figure 9. (J-H) vs. (H-K) (*left*) and K-[3.6] vs. [3.6]-[4.5] (*right*) c-c diagrams of the IRAS 19110+1045 and 19111+1048 star-forming regions. The blue circles are selected YSO candidates and black circles are non-classified ones. Not all non-classified objects are presented in these diagrams. IRA 19111+1048 source is indicated by a red triangle.

with 25″ radius and IRAS 19111+1048 with 50″ radius), objects within those areas classified as YSOs based on only the NIR c-c diagram were included in the list of YSO candidates. We selected 909 YSOs within a 6 arcmin radius. Excluding objects in two MIR–saturated regions (115 YSOs), we achieved relatively robust parameters for 431 of the 793 selected YSOs. We also performed a visual inspection of the YSO candidates in two MIR–saturated regions, because from our point of view, these objects are of the greatest interest as they are located in the immediate vicinity of the UCHIIs. Overall, the final list comprised 518 YSOs (423 with constructed SEDs and 95 YSOs in two saturated regions). The full tables of 518 selected YSOs with their NIR, MIR and FIR photometry and parameters obtained by SED fitting tool are available VizieR On-line Data Catalog[2]. The selected YSOs form dense clusters in both UCHII regions. Therefore, the low-density extended emission observed on the MIR images, which also stands out well on the dust temperature maps in both UCHII regions, may be due to the existence of the stellar clusters. Based on the data obtained by the SED fitting tool, the minimum and maximum estimated mass in the region is 1.7 and 22 $M_\odot$, respectively. Primarily, the lack of low-mass stellar objects can be explained by the large distance of the star-forming region. We were able to identify NIR counterpart of IRAS 19111+1048 source, which has 9.4±4.3 $M_\odot$ mass, 23 000±11 000 K temperature, and $(2.5\pm1.2) \times 10^6$ years evolutionary age. Unfortunately, due to the saturation of the central parts of the UCHII regions in the MIR range, we were unable to identify the YSOs associated with IRAS 19110+1045 source.

The distribution of the identified YSOs in the K versus J–K CMD is shown in the left and middle panels of Figure 10. The positions of objects in the two IRAS clusters (circles) and non-cluster objects (crosses) are different. The clusters' members and non-cluster objects exhibit low scatter relative to the isochrones. An overwhelming majority (more than 80%) of the non-cluster objects are younger than 0.1 Myr. In contrast, about 75% of objects in the IRAS clusters are older than 0.1 Myr and concentrated around the ZAMS. For improved clarity, the histograms of (J - K)$_{abs}$ are shown in the top left and middle panels. In general, the (J - K)$_{abs}$ spread of the vast majority of stellar objects from both samples is small. The distribution of evolutionary ages (by the SED fitting tool) for the non-cluster (middle right) and Control field 2 (lower right) objects has a well-defined, coincident peak and confirms the results of (J - K)$_{abs}$ histograms. In contrast, the distribution of the evolutionary ages of the objects in the clusters has two peaks (top right) which was constructed based on parameters from only 29 YSOs for which the SED fitting tool was applied. Most of the other 95 YSOs in the MIR-saturated regions are concentrated around the ZAMS and to the left of the 1 Myr isochrone. Therefore, we assumed that these objects will have a real contribution to the first peak in the evolutionary age distribution. Accordingly, this distribution will have only one well-defined peak as the histogram of (J - K)$_{abs}$. The small spread of evolutionary ages suggests that the clusters owe their origin to a triggering shock. The non-cluster YSOs are found to be uniformly distributed in the molecular cloud. Therefore, the origin of the non-cluster objects cannot be explained by the activity of the embedded massive stars in the UCHII regions. To understand the existence of the non-cluster objects, we

---

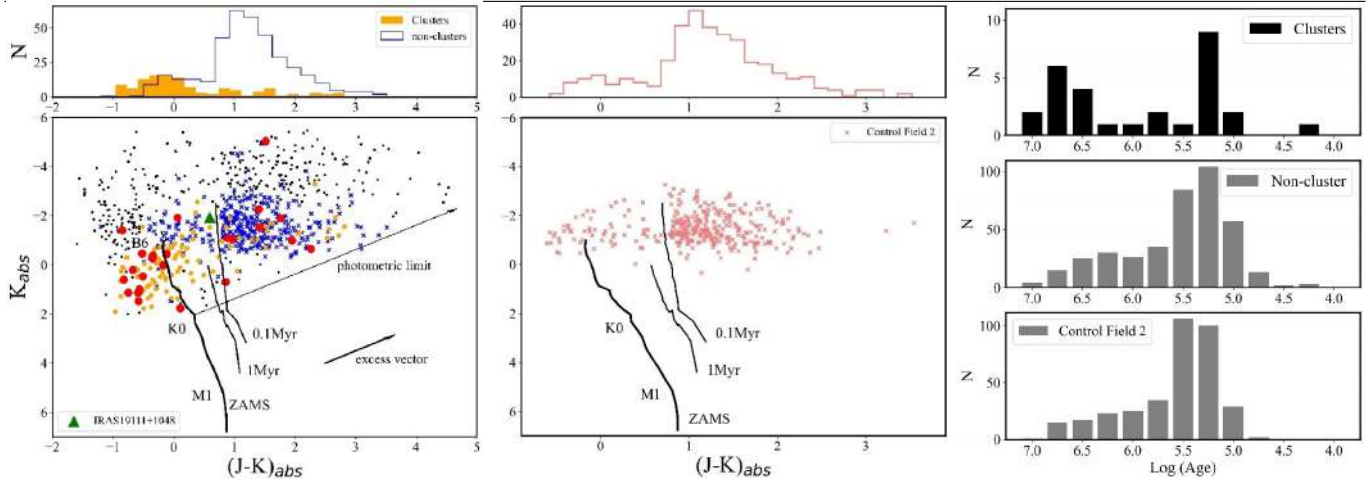[2]The full table is available in VizieR On-line Data Catalog: J/other/PASA/39.24

Figure 10. (*Bottom left and middle*) K versus (J–K) CMDs for identified YSOs in the IRAS 19110+1045 and 19111+1048 star-forming regions, and Control field 2, respectively. Red circles are stellar objects within the IRAS clusters with constructed SED. Objects located in the saturated regions are yellow circles. Non-cluster objects are blue crosses and no-SED objects are black dots. IRAS 19111+1048 source is indicated by a green triangle and labelled. Stellar objects located in Control field 2 are indicated by coral crosses. (*Top left and middle*) Histograms of (J - K)$_{abs}$ values. (*Right*) Histogram of evolutionary ages for members of the IRAS clusters (top), the non-cluster objects (middle), and the objects in the Control field 2 (bottom).

performed the same analysis in Control field 2 which is very close to the considered region. YSOs in Control field 2 show the same behavior as the non-cluster objects (evolutionary ages, masses, and surface stellar density). Accordingly, it is plausible that the non-cluster YSOs are part of the young stellar population of the GRSMC 45.46+0.05 molecular cloud. To understand the tracers of their origins, the star formation history of the GRSMC 45.46+0.05 star-forming region as a whole must be investigated.

5. Conclusion

At least for 20 regions, we obtained that around a middle- and high-mass YSO, in a certain stage of evolution, a group of young stars was formed and with modified selection criteria (depth of images, longer wavelength range), the percentage of detected groups should increase.

Below the main results of the detailed study of the selected star-forming regions are presented:

- Totally, we revealed 84 (05137+3919), 1224 (05168+3634), and 518 (19110+1045) YSOs.

- The selected YSOs are distributed nonuniformly in the IRAS 05137+3919 star-forming region and form two subgroups.

- The distribution of stars in the IRAS 05168+3634 field made it possible to reveal five dense subgroups around IRAS sources, which repeat the shape of the molecular cloud seen in FIR wavelengths. We concluded that IRAS 05168+3634 and other four sub-regions (IRAS 05184+3635, 05177+3636, 05162+3639, and 05156+3643) are embedded in the single molecular cloud and based on *Gaia* EDR3 parallaxes are located at ∼1.9 kpc distance.

- The age spread of the IRAS 05137+3919 and IRAS 05168+3634 star-forming regions is much larger, and, therefore, it can be concluded that the stellar population is formed as a result of independent condensations in the parent molecular cloud.

- The presence of a region (bridge) with relatively high density and low temperature positioned between the G45.12+0.13 and G45.07+0.13 UC HII regions suggests that these UC HII regions are physically connected.

- The IRAS clusters' members in G45.12+0.13 and G45.07+0.13 UC HII regions exhibit low scatter relative to the isochrones and their evolutionary age distribution shows small spread. Therefore, we concluded that their origin can be relate to an external triggering shock.

- Among considered star-forming regions, massive stars were detected only in the region where star formation was probably triggered, that are IRAS 19110+1045 and 19111+1048

- We assumed that uniformly distributed non-cluster YSOs in the region surrounding IRAS 19110+1045 and 19111+1048 are part of the young stellar population of the GRSMC 45.46+0.05 molecular cloud.

- The distribution of classified YSOs in the field showed that Class II objects are distributed more homogeneously on the field than Class I objects, which are located in certain areas and show clear concentrations. This confirms the assumption that, unlike the Class II objects, Class I objects did not have enough time to leave their birthplaces after formation.

Acknowledgements

References

Ambartsumian V. A., 1947, The evolution of stars and astrophysics

Azatyan N. M., 2019, Astron. Astrophys. , 622, A38

Azatyan N. M., Nikoghosyan E. H., 2018, Communications of the Byurakan Astrophysical Observatory, 65, 228

Azatyan N. M., Nikoghosyan E. H., Khachatryan K. G., 2016, Astrophysics, 59, 339

Azatyan N., Nikoghosyan E., Harutyunian H., Baghdasaryan D., Andreasyan D., 2020, Communications of the Byurakan Astrophysical Observatory, 67, 211

Azatyan N., Nikoghosyan E., Harutyunian H., Baghdasaryan D., Andreasyan D., 2022, Proc. Astron. Soc. Aust. , 39, e024

Carey S. J., et al., 2009, Publ. Astron. Soc. Pac. , 121, 76

Churchwell E., et al., 2009, Publ. Astron. Soc. Pac. , 121, 213

Cutri R. M., et al., 2003, VizieR Online Data Catalog, p. II/246

Faustini F., Molinari S., Testi L., Brand J., 2009, Astron. Astrophys. , 503, 801

Fazio G. G., et al., 2004, Astrophys. J. Suppl. Ser. , 154, 10

González-Samaniego A., Vazquez-Semadeni E., 2020, Mon. Not. R. Astron. Soc. , 499, 668

Griffin M. J., et al., 2010, Astron. Astrophys. , 518, L3

Lada C. J., Lada E. A., 2003, Ann. Rev. Astron. Astrophys. , 41, 57

Lucas P. W., et al., 2008, Mon. Not. R. Astron. Soc. , 391, 136

Molinari S., et al., 2016, Astron. Astrophys. , 591, A149

Neugebauer G., et al., 1984, Astrophys. J. Lett. , 278, L1

Nikoghosyan E. H., Azatyan N., 2014, Astrophysics, 57, 330

Nikoghosyan E., Azatyan N., Harutyunian H., Baghdasaryan D., Andreasyan D., 2020, Communications of the Byurakan Astrophysical Observatory, 67, 187

Nikoghosyan E. H., Azatyan N. M., Andreasyan D. H., Baghdasaryan D. S., 2021, Astrophys. Space. Sci. , 366, 114

Pilbratt G. L., et al., 2010, Astron. Astrophys. , 518, L1

Poglitsch A., et al., 2010, Astron. Astrophys. , 518, L2

Preibisch T., 2012, Research in Astronomy and Astrophysics, 12, 1

Price S. D., Egan M. P., Carey S. J., Mizuno D. R., Kuchar T. A., 2001, Astron. J. , 121, 2819

Robitaille T. P., Whitney B. A., Indebetouw R., Wood K., 2007, Astrophys. J. Suppl. Ser. , 169, 328

Soderblom D. R., 2010, Ann. Rev. Astron. Astrophys. , 48, 581

Stahler S. W., Palla F., 2005, The Formation of Stars

Varricatt W. P., Davis C. J., Ramsay S., Todd S. P., 2010, Mon. Not. R. Astron. Soc. , 404, 661

Wright E. L., et al., 2010, Astron. J. , 140, 1868